
Article:
Sharma, Mahima orcid.org/0000-0003-3960-2212, Abayakoon, Palika, Lingford, James P et al. (6 more authors) (2020) Dynamic structural changes accompany production of dihydroxypropanesulfonate by sulfolactaldehyde reductase. ACS Catalysis. ISSN 2155-5435

https://doi.org/10.1021/acscatal.9b04427

ACS Catalysis

Article

Dynamic structural changes accompany the production of dihydroxypropanesulfonate by sulfolactaldehyde reductase

Mahima Sharma, Palika Abayakoon, James P Lingford, Ruwan Epa, Alan John, Yi Jin, Ethan D. Goddard-Borger, Gideon J. Davies, and Spencer J. Williams

ACS Catal., **Just Accepted Manuscript** • DOI: 10.1021/acscatal.9b04427 • Publication Date (Web): 30 Jan 2020

Just Accepted

is published by the American Chemical Society. 1155 Sixteenth Street N.W., Washington, DC 20036

Dynamic Structural Changes Accompany the Production of Dihydroxypropanesulfonate by Sulfolactaldehyde Reductase

Mahima Sharma,[†] Palika Abayakoon,[‡] James P. Lingford,[§] Ruwan Epa,[‡] Alan John,[§] Yi Jin,[†,¶] Ethan D. Goddard-Borger,[*,§] Gideon J. Davies,[*,†] Spencer J. Williams[*,‡]

Author Affiliations

[†]York Structural Biology Laboratory, Department of Chemistry, University of York, Heslington, YO10 5DD, U.K.

[‡]School of Chemistry and Bio21 Molecular Science and Biotechnology Institute and University of Melbourne, Parkville, Victoria 3010, Australia

[§]ACRF Chemical Biology Division, The Walter and Eliza Hall Institute of Medical Research, Parkville, Victoria 3010, Australia and Department of Medical Biology, University of Melbourne, Parkville, Victoria 3010, Australia

[¶]Current address: School of Chemistry, Cardiff University, Park Place, Cardiff CF10 3A

*sjwill@unimelb.edu.au, goddard-borger.e@wehi.edu.au, gideon.davies@york.ac.uk

Abstract

2,3-Dihydroxypropanesulfonate (DHPS) is a major sulfur species in the biosphere. One important route for the production of DHPS is sulfoglycolytic catabolism of sulfoquinovose (SQ) through the Embden-Meyerhof-Parnas (sulfo-EMP) pathway. SQ is a sulfonated carbohydrate present in plant and cyanobacterial sulfolipids (sulfoquinovosyl diacylglyceride and its metabolites) and is biosynthesised globally at a rate of around 10 billion tonnes per annum. The final step in the bacterial sulfo-EMP pathway involves reduction of sulfolactaldehyde (SLA) to DHPS, catalysed by an NADH-dependent SLA reductase. Based on conserved sequence motifs, we assign SLA reductase to the β-hydroxyacid dehydrogenase (β-HAD) family, an example of a β-HAD enzyme that acts on a sulfonic acid substrate, rather than a carboxylic acid. We report crystal structures of the SLA reductase YihU from *E. coli* K-12 in its apo and cofactor-bound states, as well as a ternary complex YihU•NADH•DHPS with the cofactor and product bound in the active site. Conformational flexibility observed in these structures, combined with kinetic studies, confirm a sequential mechanism and provide evidence for dynamic domain movements that occur during catalysis. The ternary complex structure reveals a conserved sulfonate pocket in SLA reductase that recognises the sulfonate oxygens through hydrogen bonding to Asn174, Ser178, and the backbone amide of Arg123, along with an ordered water molecule. This triad of residues distinguishes these enzymes from classical β-HADs that act on carboxylate substrates. A comparison of YihU crystal structures with close structural homologues within the β-HAD family highlights key differences in the overall domain organization and identifies a peptide sequence that is predictive of SLA reductase activity.

Keywords: sulfoglycolysis, X-ray crystallography, alkylsulfonate, NADH-dependent, reductase, three-dimensional structure, bisubstrate enzyme kinetics

Graphical abstract

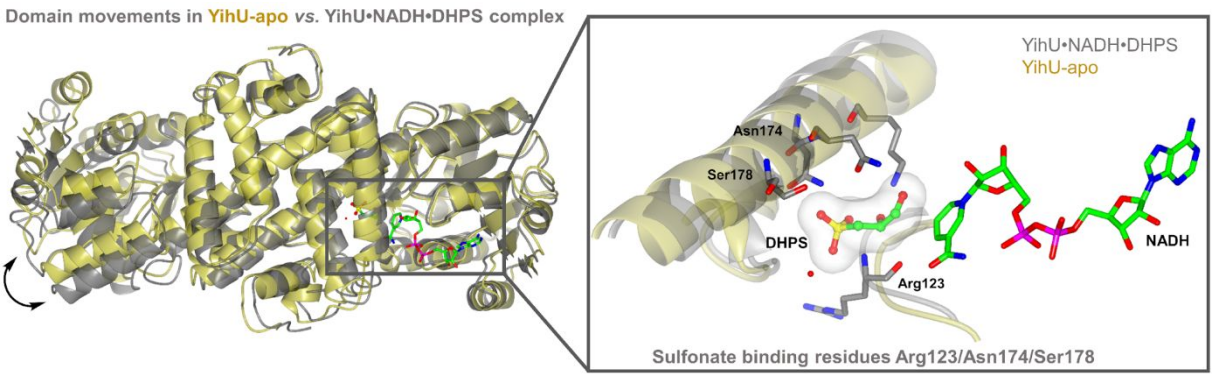
Domain movements in YihU-apo vs. YihU•NADH•DHPS complex
YihU•NADH•DHPS
YihU-apo
Asn174
Ser178
DHPS
Arg123
NADH
Sulfonate binding residues Arg123/Asn174/Ser178

The biodegradation of organosulfur compounds within the biogeochemical sulfur cycle is crucial for recycling this essential macronutrient. 2,3-Dihydroxypropanesulfonate (DHPS) is an important intermediate in the biosulfur cycle and is produced globally on a significant scale from organosulfur precursors by plants, diatoms and bacteria. Bacteria produce DHPS by catabolism of the sulfosugar sulfoquinovose (SQ), which has an estimated annual production of 10^{10} tonnes, through the sulfoglycolysis pathway (Figure 1).[1-2] DHPS is also a major species in sulfur fluxes through the marine web. Oceanic diatoms produce massive amounts of DHPS, presumably by deamination of cysteinolic acid,[3-5] with production levels on par with the major marine organosulfur species dimethylsulfoniopropionate[6,7] and dimethylsulfoxonium propionate.[8] DHPS is the substrate for a range of bacterial biomineralization processes that cleave the carbon-sulfur bond to liberate inorganic sulfite,[3] sulfate[9] or sulfide,[10] or that lead to assorted secondary metabolites.[11] For instance, *Desulfovibrio sp.* strain DF1 from anaerobic sewage sludge converts DHPS to hydrogen sulfide,[10] while Roseobacter in marine environments convert DHPS to bisulfite.[12,13] To facilitate these processes, enzymes have evolved to catalyse the inversion of *R*-DHPS, which may represent the stereoisomer formed by deamination of cysteinolic acid, to *S*-DHPS.[12] On the whole, the enzymes and pathways involved in the synthesis and degradation of this significant sulfur-containing metabolite have not been well studied.

The molecular cloning of the sulfoglycolytic Embden-Meyerhof-Parnas (sulfo-EMP) pathway responsible for catabolism of SQ in *E. coli* revealed that the final chemical step involved reduction of the C_3-sulfonate sulfolactaldehyde (SLA) to DHPS by the NADH-dependent reductase YihU, followed by export from the cell.[1] YihU belongs to the β-hydroxyacid dehydrogenase family (β-HADs), a group of enzymes that until the discovery of the SLA reductase activity of YihU were believed to act exclusively on 3-hydroxy carboxylic acid substrates, such as glycerate, 6-phosphogluconate, serine, D-phenylserine, 2-(hydroxymethyl)glutarate and succinate semialdehyde (an earlier report anticipated this result by noting the YihU catalysed NADH-dependent oxidation of 3-hydroxypropanesulfonate).[14] β-HADs feature highly conserved structural folds and conserved sequence motifs for cofactor and substrate binding.[15] β-HADs bind their substrates in a cleft formed between their two domains: an N-terminal Rossmann domain and an all-helical C-terminal dimerization domain. Recently, the 3D structure of a NADPH-dependent dehydrogenase (IsfD) that plays a role in nitrogen assimilation from taurine (aminoethyl sulfonate) was reported.[16] IsfD belongs to the short-chain dehydrogenase/reductase family and catalyses the reduction of sulfoacetaldehyde (SA) to isethionate: this enzyme utilizes a Tyr-Arg-Gln motif to recognize the sulfonate group of these C_2-organosulfonates. IsfD differs from β-HADs in its two-domain structural framework and contains an N-terminal Rossmann fold and a small C-terminal tail formed of two β-strands.

Another group of NADH-dependent SA reductases have been identified from *Bilophila wadsworthia* (SarD)[17] and *Bifidobacterium kashiwanohense* (TauF)[18] that belong to the metal-dependent alcohol dehydrogenase superfamily.

In this work, we present a combined sequence, kinetic and structural study of SLA reductase (YihU) from *E. coli* str. K-12. Sequence analysis reveals YihU to be the first example of a β-HAD that acts on a sulfonic acid substrate and identifies a sequence motif conserved among SLA reductases. A biochemical assay established to assess the kinetic properties of YihU confirms that it is a dedicated SLA reductase, with no detectable activity on the analogous glycolytic intermediate glyceraldehyde-3-phosphate. We show that modified NADH analogues are inhibitors of YihU, and that the enzyme acts through a rapid equilibrium sequential mechanism. Finally, we present a series of 3-D X-ray structures of YihU in its apo form, in a binary complex with NADH, and in a ternary product-like complex, YihU•NADH•DHPS. The 3-D structures provide a structural basis for cofactor binding and sulfonate recognition and illuminate the dynamic structural changes that occur during catalysis.

Results and Discussion

Sequence alignment reveals YihU belongs to the β-HAD family. Alignment of the *E. coli* YihU sequence with that of characterized β-hydroxyacid dehydrogenases (β-HADs) reveals that it shares the four defining motifs that are collectively involved in cofactor-binding, substrate-binding and catalysis (Figure 2A).[15] Motif-1 of β-HADs consists of *GXXGXGXMGXXXAXNXXXXG* and contains the dinucleotide cofactor binding residues; motif-2 consists of substrate-binding sequence *DAPV**SGG**XXXAXXG*; motif-3 consists of *GXXGXGXXX**K**XXXN/Q*, which contains the active site lysine and conserved Asn/Gln residue; and motif-4 derives from the C-terminal domain comprising *KDLGXAXD* sequence and shows a high degree of conservation among bacterial homologues. Examination of the sequence alignment of a phylogenetically-related putative SLA reductases (assigned based on context within gene clusters encoding the sulfo-EMP pathway) from a selection of alpha-, beta- and gammaproteobacteria along with other β-HADs including 3-hydroxyisobutyrate dehydrogenases, 2-hydroxymethylglutarate dehydrogenases, 2-hydroxyl-3-oxopropionate reductases, and tartronate semialdehyde reductases, shows that SLA reductases form a distinct sub-group within the β-HAD family. The sequence alignment reveals that the key differences in the YihU sequences lie within motif-2 where Gly122-Arg123-Thr124 replace the conserved Ser-Gly-Gly seen in β-HADs (Figure 2B). Based on these sequence alignments that reveal the putative SLA reductases form a distinct subgroup, we define an extended motif-

2 [*D/EVPV**GRT**XXXAXXG*] as a 'sulfonate substrate-binding motif' common to all SLA reductases.

YihU SLA reductase does not reduce GAP and follows a rapid equilibrium sequential kinetic mechanism. Reaction rates for YihU catalysed conversion of racemic D/L-SLA[19] to DHPS were measured by monitoring absorbance at 340 nm for enzymatic NADH oxidation to NAD^+. By varying the concentration of D/L-SLA and keeping NADH constant (0.10 mM) or *vice versa* using constant D/L-SLA (5.00 mM), we could perform Michaelis-Menten kinetic analyses for the two substrates. Kinetic parameters were calculated for the concentration of D-SLA, assuming that L-SLA was not a substrate. Both NADH and SLA exhibited saturation kinetics, allowing calculation of k_{cat}, K_M^{app} and k_{cat}/K_M^{app} values under pseudo first order conditions (Figure 3A,B). At [NADH] = 0.1 mM, under conditions of varying [SLA] we determined K_M^{app} = 0.3 mM, k_{cat} = 3.3 x 10^2 s^{-1}, and k_{cat}/K_M^{app} = 1.09 x 10^3 mM^{-1} s^{-1}. At [D-SLA] = 2.5 mM, under conditions of varying [NADH] we determined K_M^{app} = 0.082 mM, k_{cat} = 5.48 x 10^2 s^{-1}, and k_{cat}/K_M^{app} = 6.72 x 10^3 mM^{-1} s^{-1} (for full data and associated errors see Table 1). No activity was observed for reduction of racemic glyceraldehyde phosphate (GAP)[20] under similar conditions. GAP is produced from DHAP through the action of triose phosphate isomerase, and in the first step of lower glycolysis undergoes conversion to 1,3-bisphosphoglycerate by the action of GAP dehydrogenase (GADPH). The lack of activity of YihU on GAP prevents interference with this important glycolytic/gluconeogenic intermediate. Saito *et al.* reported that YihU catalyzes succinate semialdehyde reduction with kinetic parameters of V_{max} = 0.20±0.04 mmol min^{-1} mg^{-1} and K_M^{app} = 4.3±1.2 mM (at 1 mM NADH),[14] which we calculate equates to k_{cat}/K_M^{app} = 26±12 M^{-1} s^{-1}. Thus, YihU exhibits a 42,000-fold greater catalytic efficiency for the reduction of SLA over SSA. Collectively, these data confirm that YihU is a dedicated SLA reductase.

Multi-substrate enzymes perform catalysis through two main mechanisms: the sequential (ternary complex) mechanism, in which both substrates must bind before a chemical step leading to product formation; or the ping-pong mechanism, in which one or more products are released prior to binding of all substrates. The Theorell-Chance mechanism is a special case in which there is a defined order of substrate association and product release without accumulation of a ternary complex. As SLA reductase has two substrates and two products, its molecularity is described as Bi-Bi. For β-HADs[21] and other dehydrogenases,[22,23] a sequential Bi-Bi mechanism is often reported with the binding of the redox-active cofactor preceding localisation and binding of the substrate.

For a bisubstrate enzyme with substrates A and B, plotting $1/v_0$ versus 1/[A] at various constant concentrations of substrate B or $1/v_0$ versus 1/[B] at various constant concentrations of substrate A can indicate the mechanism of the reaction.[24] For a ping-pong mechanism, plotting $1/v_0$ versus 1/[A] affords a series of straight lines with slope of $K_M(A)/V_{max}$. In contrast, for a classical sequential mechanism plotting $1/v_0$ versus 1/[A] will produce a family of straight lines with slope depending on the concentration of B that intersect to the left of the *y*-axis, or in the case of a rapid equilibrium sequential mechanism, on the *y*-axis.[25] To study the kinetic mechanism used by YihU we simultaneously varied the concentration of SLA while NADH was held at saturation ([NADH] = 0.05-0.30 mM) and *vice versa* ([D/L-SLA] = 2.50-12.0 mM), at a constant concentration of YihU. The resulting double-reciprocal plots yielded patterns of lines that intersected on the *y*-axis (Figure 3C,D). For the plot of 1/[NADH] (at different SLA concentrations) the data intersected the *y*-axis above zero; for the plot of 1/[SLA] (at different NADH concentrations) the data clearly intersects on the origin. These patterns directly rule out a ping-pong mechanism for YihU. While intersection on the y-axis is unusual, it has been reported for creatine kinase by Schimerlik and Cleland, who derived the corresponding kinetic equations, and showed that the data could indicate which substrate bound first.[25] In line with the analysis of Schimerlik and Cleland, the patterns observed here are consistent with a rapid equilibrium sequential mechanism, and indicate initial binding of NADH. The kinetic mechanism allows proposal of a catalytic mechanism for SLA reductases that is consistent with that proposed for other β-HADs and involves ordered binding of the two substrates NADH and SLA to form a ternary complex, followed by a chemical step involving hydride transfer from NADH and protonation of the substrate.

We synthesized two NADH analogues by partial (tetrahydro-NADH) and complete reduction (hexahydro-NADH) of the nicotinamide ring of NADH, as described by Dave *et al*.[26] and assessed these compounds as inhibitors of YihU. Owing to the small amounts of these compounds available we limited our studies to determination of IC_{50} values. Under conditions of [SLA] = K_M(SLA)/10 and [NADH] = K_M(NADH) we measured IC_{50} values of 4.03 and 10.3 mM, respectively (Figure S1). These data reveal that tetrahydro-NADH is a better inhibitor than hexahydro-NADH, as might be expected considering its greater structural resemblance to the cofactor. Disappointingly, we were unable to obtain X-ray structures of these inhibitors bound to YihU.

YihU forms a dimer of intimate homodimer pairs. In order to identify the amino acid residues involved in substrate binding and catalysis, we solved the X-ray structure of YihU. Despite conserved sequence motifs and moderate sequence similarity with other β-HADs, we could not achieve a structure solution using a single model. The YihU structure was solved

using the molecular replacement pipeline BALBES[27] that selected a human hydroxyisobutyrate dehydrogenase as the reference structure (PDB ID 2GF2 with 31% sequence similarity). Data collection and refinement statistics for YihU structures are given in Table S1. YihU crystallised as a dimer of dimers with four molecules present in the asymmetric unit (Figure 4A). Size exclusion chromatography-multiangle light scattering (SEC-MALS) confirmed that YihU also exists as tetramer in solution (Figure S2). Within the asymmetric unit, each protomer adopts a two-domain architecture containing a N-terminal nucleotide binding domain (residues 1-164) and a C-terminal helical bundle (residues 165-294) both connected by long inter-domain helix α8 (Figure S3). The N-terminal domain is composed of a classical α/β Rossmann fold (comprised of an extended sheet formed of β1-6, flanked by α1-5 in a three-layered sandwich) appended with an additional β-α-β motif containing β7-9 and α6-7. An intimate homodimer pair between two monomers is formed through 3D domain swapping of the dimerization domains involving C-terminal helices α8-14. This dimerization domain is formed when the central trans-domain helix α8 from one monomer (A) inserts into the C-terminal helical bundle from the opposite monomer (B) making several reciprocal interactions through both charged and hydrophobic residues (Figure S4).

The tetrameric assembly and domain organization of YihU matches that of imine reductases (IREDs). Four interfaces are present within the subunits of the YihU tetramer: A-B (Interfaces I and II), A-C (Interface III) and A-D (Interface IV) (Figure 4A, Figure S5). PISA analysis of the AB dimer assembly indicated a total buried surface area of 10,638 Å^2. The interface area for chains A-B is 4,023 Å^2, which corresponds to 38% of the total, indicating an intimate homodimer pair. At the major interface, interface I, the C-terminal bundle of subunit A (shown in grey) interacts with C-terminal domain of subunit B to form a hydrophobic helical core. Interface II also occurs in the AB dimer and harbours the active site formed by reciprocal domain sharing between C-terminal helices (A) and the N-terminal Rossmann domain of chain B, indicating that dimer assembly is essential for catalytic activity of YihU. Conserved residue Lys171 in motif-3 projects into an inter-domain cleft that is lined mainly by charged, polar residues (Table S2). Interfaces III and IV comprise minor interfaces and are formed by hydrogen bonding interactions between subunits A-C and A-D, respectively. These interfaces appear to be important for assembly of the tetramer and may contribute to the overall stability of the enzyme.

A DALI search using YihU against the RCSB PDB library revealed that its closest structural neighbours belong to the β-HAD family. The closest structural homologues included human 3-hydroxyisobutyrate dehydrogenase (PDB ID: 2GF2 with DALI z score of 31.6, rmsd 2.2 and 31% sequence ID), tartronate semialdehyde reductase from *Salmonella*

typhimurium LT2 (1VPD[28] with DALI z score of 31.5 and 32% sequence ID) and 6-phosphogluconate dehydrogenase from *Pyrobaculum calidifontis* (3W6U[29] with z score of 31.4 and 31% sequence similarity). Several other annotated hydroxyisobutyrate dehydrogenases (HIBDHs) that have been reported to reduce imine substrates (imine reductases or IREDs) were also identified including 5OCM,[30] 5G6S,[31] and 6EOD[32] with low sequence identity (16-20%) but relatively high DALI z scores of 25-27 and overall rmsd of 2.2-3.2, reflecting high structural similarities. Superposition of monomers of human HIBDH (2GF2) and the IRED from *Streptosporangium roseum* (5OCM) with YihU shows all three proteins contain a common two-domain structure comprising N-terminal Rossmann-like fold and C-terminal helical bundle connected by a long transdomain helix. However, while superposition of the isolated Rossmann domain and C-terminal helices of YihU monomer over the two domains of human HIBDH shows high fold conservation (RMSD 1.14Å/160 residues and 1.32Å/74 residues for N- and C-termini domains, respectively), the quaternary organization of the subunits display large differences. In human HIBDH, α9 helix of C-terminal domain takes a sharp turn to interact with N-terminal domain from the same monomer. As a result, the two monomers in human HIBDH sit adjacent to one another and only interact along the length of long α8 helix, arranged in a back-to-back fashion in a dimer pair (Figure 4B). On the other hand, the two domains in YihU are rewired such that their subunit organization is similar to IREDs.[33] YihU and IREDs possess homodimeric folds formed by extensive domain swapping. In YihU (or the equivalent helix in IREDs), helix α9 of monomer A adopts an extended conformation so that the C-terminal helices (of chain A) travel further away and form an active site cleft with the N-terminal domain of opposite monomer B (Figure 4C, Figure S6).

A binary YihU•NADH complex reveals dynamic domain movement upon cofactor binding. Co-crystallization of YihU with NADH afforded a binary complex showing clear density for the cofactor bound to the N-terminal Rossmann domain of all four monomers within the asymmetric unit (Figure 5A-B, Figure S7). Domain conformational motion analyses of the apo and YihU•NADH structures, using the DynDom program,[34] reveals the former adopts an 'open' and the latter a 'closed' conformation, as a result of two dynamic domains with a bending region comprised of residues 156-166 connecting the two domains. Cofactor binding results in an 8° inter-domain rotation to form a more compact active-site pocket that encapsulates the NADH molecule. The NADH molecule binds in a *syn* conformation and the 2'-hydroxyl of ribose ring is hydrogen-bonded to Asp31, a residue that provides specificity for NADH. By contrast, NADPH binding β-HAD homologues possess Asn at this position, usually followed by an arginine residue that makes stacking interactions with adenine and binds to 2'-phosphate of NADPH. The structure shows that NADH specificity likely arises from destabilizing interactions of Asp31 that would occur with the 2'-phosphate in NADPH. The

nicotinamide ring of NADH projects into a relatively narrow cleft formed as a result of domain closure upon binding of the cofactor.

YihU possesses a defined substrate channel for entry of SLA to the active site. Two pores that could possibly provide for entry of SLA into the active site (as defined by the location of the catalytic Lys171) were identified in the YihU-apo structure. However, upon binding of NADH to form the YihU•NADH complex, domain movement leads to closure of the active site, blocking one of these pores. At the entry to the other pore, Arg123 (chain A) and Lys213 (chain B) contribute to a positively charged surface patch which may facilitate entry of the negatively charged substrate SLA (Figure 5C).

Using CAVER Web 1.0,[35] a tool for visualization and analysis of tunnels and channels in protein structures, we selected Lys171 in the YihU•NADH structure as the reference starting point. A 10.4 Å long tunnel was visualised, which could provide a pathway for entry of the substrate SLA (and possibly release of the product DHPS). This tunnel tapers to a bottleneck at the back of the sulfonate-binding pocket to confine the dimensions of the substrate pocket (Figures S8-9). Thus, the residues forming the sulfonate binding pocket, the residues at the entry to this predicted tunnel, and its size may contribute to the substrate specificity of YihU, possibly involving electrostatic filtering of anionic substrates at the entrance to the tunnel (Table S2).

A ternary YihU•NADH•DHPS complex reveals the sulfonate binding pocket and active site residues. A ternary complex was obtained with NADH and the product DHPS, by soaking solid racemic DHPS directly onto a YihU•NADH crystal in mother liquor. Close examination of the 3D structure revealed the two dimer pairs (comprised of four chains in the asymmetric unit) are present in different conformations with varying ligand densities observed close to Ser178/Asn174 in the active site cleft. The NADH cofactor was found to be somewhat mobile in the different chains in the structure upon soaking DHPS at high concentrations, resulting in apo conformations in two chains and a binary YihU•DHPS complex in one of the chains. In one monomer, clear density was seen for both the NADH cofactor and another ligand bound at the active site that allowed modelling of the natural isomer *S*-DHPS (Figure 6A). *S*-DHPS sits within the active site and is anchored to Lys171 by hydrogen-bonds to C-1 (2.5 Å) and C-2 (2.9 Å) hydroxyls, and flanked by bulky, hydrophobic residues on the other side (Phe233 and Trp279 from the opposite subunit B). A well-ordered binding pocket surrounds the sulfonate group of *S*-DHPS. One sulfonate oxygen makes hydrogen bonds with Ser178 and Asn174 at 2.6 and 3.1 Å, respectively; the second oxygen is hydrogen-bonded to Asn174 (2.9 Å) and the backbone amide N-H of Arg123 (2.9 Å); and the third sulfonate oxygen makes a

hydrogen bond with the bound water molecule (Figure 6B). This water molecule is 3 Å from the backbone amide of Ala210 (not a conserved residue) and at 2.7 Å and 3.3 Å distance from two ordered water molecules; one of these H-bonds to side-chain hydroxyl of Ser219. Crucially, this sulfonate binding triad of residues Arg123-Asn174-Ser178 is conserved in all assigned bacterial SLA reductases (Figure 2A).

While *S*-DHPS is the product of the reaction, within the YihU•NADH•DHPS complex NADH and *S*-DHPS are positioned in what can be considered a catalytically relevant conformation, with C-1 of DHPS situated 3.3 Å away from C4 of nicotinamide ring. As D-SLA would make many of the same interactions as *S*-DHPS and NADH is seen bound in a *syn* conformation in our ternary complex, this confirms that reduction of SLA by NADH will involve transfer of hydride from the *si*-face of NADH (Figure 6C).

Identification of the structural basis for binding of sulfonate and carboxylate substrates in the β-HAD family. In order to understand how sulfonate/carboxylate selectivity arises within the β-HAD family, we compared the structures of the YihU•NADH•DHPS complex and that of *Salmonella typhimurium* GarR-tartronate semialdehyde reductase bound to a substrate analog, L-tartrate.[28] A key difference is visible within motif-2, which contains the substrate binding loop that interacts with the carboxylate/sulfonate groups of the ligands (Figure 7). In YihU, Arg123 within the triplet Gly122-Arg123-Thr124 interacts with one sulfonate oxygen, whereas in GarR the equivalent (and conserved among classical carboxylate β-HADs) Ser123-Gly124-Gly125 residues exhibit a 180° flip in the central glycine (possibly enabled by the conformationally flexible Cα backbone of the two glycines) allowing one carboxylate oxygen to bind the backbone amides of Gly124 and Gly125, present at 2.7 Å and 2.9 Å respectively, and the other carboxylate oxygen to hydrogen-bond to side-chain hydroxyl of Ser123 (2.6 Å).

We used site-directed mutagenesis to explore the role of the sulfonate binding motif in the function of YihU. Amino acids in the triplet Gly122-Arg123-Thr124 were individually converted to the corresponding residue in GarR and Michaelis-Menten parameters of the resulting variant proteins were measured under pseudo-first order conditions (Figure S11). All mutant enzymes suffered a reduction of catalytic efficiency (k_{cat}/K_M^{app}). The change in k_{cat}/K_M^{app} for NADH at constant [SLA] for each of the mutants versus the wildtype was small, in the range of 3-12-fold reduction, consistent with the sites of mutation involving interaction with SLA (Table 1). Conversely, the change in k_{cat}/K_M^{app} for SLA at constant [NADH] for each of the mutants relative to wildtype was greater, comprising a 25-, 130- and 230-fold reduction for the

G122S, R123G and T124G mutants, respectively. For the three mutants, K_M^{app} for SLA at constant [NADH] was increased versus wildtype.

Conclusion

As the final step in the sulfo-EMP pathway, the NADH-dependent SLA reductase YihU is an important enzyme in sulfur cycling in the biosphere. Our data reveals that YihU acts specifically on SLA, supporting an exclusive role in the *E. coli* sulfo-EMP pathway in reduction of SLA to the excreted metabolite DHPS. Absence of activity on GAP shows that YihU is unlikely to interfere with lower glycolysis or gluconeogenesis. A previous study by Saito *et al.* using recombinant *E. coli* YihU revealed that this enzyme possessed succinate semialdehyde reductase activity,[14] however, our data shows that it possesses a 42,000-fold preference for SLA in terms of k_{cat}/K_M. Indeed, since the sulfo-EMP gene cluster is overexpressed when *E. coli* is grown on SQ,[1] reduction of SSA is not only catalytically insignificant but may also be physiologically unimportant. Interestingly, Saito *et al.* demonstrated that 3-hydroxypropanesulfonate could be oxidized by YihU in the presence of NAD^+.[14] While 3-hydroxypropanesulfonate is not a naturally occurring metabolite, it is the 2-deoxy analogue of DHPS and so this observation foreshadowed the subsequent discovery of the role of YihU in sulfoglycolysis. Our kinetic data demonstrates a rapid equilibrium sequential mechanism. The acquisition of YihU•NADH binary and YihU•NADH•DHPS ternary crystal complexes are consistent with a sequential mechanism involving initial binding of NADH. Binding of a sulfonate substrate occurs through a triad of conserved residues (Arg123-Asn174-Ser178) common to all putative SLA reductases. It is only known in one other case how enzymes in the sulfo-EMP pathway recognize a sulfonate group: 3-D structures of sulfoquinovosidases that catalyze hydrolysis of SQ glycosides revealed a highly conserved Tyr-Arg-Trp triad.[36,37]

YihU possesses the four characteristic motifs that define members of the β-HAD family,[15] and represents the first β-HAD that acts on a β-hydroxysulfonic acid, rather than a β-hydroxycarboxylic acid. We identified an SLA-specific sequence *DVPV**GRT*** within motif-2 that distinguished putative SLA reductases from classical β-HADs. In the YihU•NADH•DHPS complex, a hydrogen bond between one of the sulfonate oxygens and the backbone N-H of Arg123 (within the triplet Gly122-Arg123-Thr124) appears particularly important. Conversely, in the case of tartronate reductase GarR, recognition of a carboxylate substrate is achieved by backbone chain flipping in the equivalent sequence triplet Ser123-Gly124-Gly125, resulting in a fundamentally different binding mode of the carboxylate involving side-chain hydrogen bonding with Ser123 and backbone N-H interactions with Gly124 and Gly125. Kinetic analysis of mutant enzymes created by converting each residue with the Gly122-Arg123-Thr124 triplet

of YihU to the corresponding residues in the Ser123-Gly124-Gly125 triplet of GarR are consistent with the roles of these residues in binding the sulfonate of SLA.

SLA reductases possess a close sequence relationship with hydroxyisobutyrate dehydrogenases (HIBDHs) within the β-HAD family. However, analysis of the domain arrangement seen in 3D X-ray structures highlights an alternative wiring pattern and a closer structural resemblance to imine reductases (IREDs), a sub-group of NADPH-dependent dehydrogenases that can reduce imines to amines. As seen in IREDs,[30-33] extensive swapping of C-terminal helical bundles between the YihU protomers results in an active site formed at the inter-domain cleft of a dimer pair. Examination of monomeric (1VPD, a model β-HAD) and quaternary domain-swapped (YihU) conformations reveals that while consensus sequence motifs and the overall monomer topology of β-HADs are retained, the substrate-binding motif-2 and catalytic motif-3 from opposite monomer partners in the YihU dimer pair make H-bonding interactions with the sulfonate and facilitate the binding of the natural substrate. Modelling allowed identification of a tunnel leading to the DHPS-binding subsite, and hint at a possible electrostatic gating mechanism for achieving substrate selectivity by positively charged surface residues (Arg123 and Lys213, also from opposite monomers) present at the tunnel entrance.

Because SQ is a major organosulfur species produced by essentially all photosynthetic organisms, its biomineralization is a major contributor to the global sulfur cycle. As one of just two known pathways for catabolism of SQ (the other consisting of the sulfoglycolytic Entner-Doudoroff pathway that leads to sulfolactate),[38] the sulfo-EMP pathway is important for sulfur cycling and for production of DHPS for downstream biomineralization by other members of the bacterial community. The insights provided here into the kinetics, structure and function of SLA reductases deepen our understanding of this important arm of the biogeochemical sulfur cycle and will support future bioinformatic analysis of these enzymes.

Associated content

The Supporting Information is available free of charge on the ACS Publications website at DOI: 10.1021/acschembio.xxx.

Tables S1−S2, Figures S1−S11, supporting methods on chemical synthesis procedures, cloning, protein expression and purification, enzyme kinetics, protein crystallization and X-ray crystallography and structure analysis (PDF)

Author Information

Corresponding Authors

*E-mail: sjwill@unimelb.edu.au
goddard-borger.e@wehi.edu.au
gideon.davies@york.ac.uk

ORCID

Spencer J. Williams: 0000-0001-6341-4364

Ethan D. Goddard-Borger: 0000-0002-8181-9733

Gideon J. Davies: 0000-0002-7343-776X

Acknowledgements

We thank the Australian Research Council (DP180101957), The Leverhulme Trust (Grant number RPG-2017-190), the National Health and Medical Research Council (GNT1139546 and GNT1139549), and the Royal Society for the Ken Murray Research Professorship to GJD. We thank Dr. Johan P. Turkenburg and Sam Hart for assistance with X-ray data collection, and the Diamond Light Source for access to beamlines I04, i24 and I04-1 under proposal number mx-18598. We acknowledge Dr. Andrew Leech from Bioscience Technology Facility, University of York for assistance with SEC-MALS analysis.

References

(1) Denger, K.; Weiss, M.; Felux, A. K.; Schneider, A.; Mayer, C.; Spiteller, D.; Huhn, T.; Cook, A. M.; Schleheck, D. Sulphoglycolysis in *Escherichia coli* K-12 Closes a Gap in the Biogeochemical Sulphur Cycle. *Nature* **2014**, *507*, 114–117.

(2) Goddard-Borger, E. D.; Williams, S. J. Sulfoquinovose in the Biosphere: Occurrence, Metabolism and Functions. *Biochem. J.* **2017**, *474*, 827–849.

(3) Durham, B. P.; Sharma, S.; Luo, H.; Smith, C. B.; Amin, S. A.; Bender, S. J.; Dearth, S. P.; Van Mooy, B. A.; Campagna, S. R.; Kujawinski, E. B.; Armbrust, E. V.; Moran, M. A. Cryptic Carbon and Sulfur Cycling Between Surface Ocean Plankton. *Proc. Natl. Acad. Sci. USA* **2015**, *112*, 453–457.

(4) Busby, W. F.; Benson, A. A. Sulfonic Acid Metabolism in the Diatom *Navicula pelliculosa*. *Plant Cell Physiol.* **1973**, *14*, 1123–1132.

(5) Busby, W. F. Sulfopropanedial and Cysteinolic Acid in the Diatom. *Biochim. Biophys. Acta* **1966**, *121*, 160–161.

(6) Ksionzek, K. B.; Lechtenfeld, O. J.; McCallister, S. L.; Schmitt-Kopplin, P.; Geuer, J. K.; Geibert, W.; Koch, B. P. Dissolved Organic Sulfur in the Ocean: Biogeochemistry of a Petagram Inventory. *Science* **2016**, *354*, 456–459.

(7) Dickschat, J. S.; Rabe, P.; Citron, C. A. The Chemical Biology of Dimethylsulfoniopropionate. *Org. Biomol. Chem.* **2015**, *13*, 1954–68.

(8) Thume, K.; Gebser, B.; Chen, L.; Meyer, N.; Kieber, D. J.; Pohnert, G. The Metabolite Dimethylsulfoxonium Propionate Extends the Marine Organosulfur Cycle. *Nature* **2018**, *563*, 412–415.

(9) Denger, K.; Huhn, T.; Hollemeyer, K.; Schleheck, D.; Cook, A. M. Sulfoquinovose Degraded by Pure Cultures of Bacteria with Release of C3-organosulfonates: Complete Degradation in Two-Member Communities. *FEMS Microbiol. Lett.* **2012**, *328*, 39–45.

(10) Burrichter, A.; Denger, K.; Franchini, P.; Huhn, T.; Müller, N.; Spiteller, D.; Schleheck, D. Anaerobic Degradation of the Plant Sugar Sulfoquinovose Concomitant with H_2S Production: Escherichia coli K-12 and Desulfovibrio sp. Strain DF1 as Co-culture Model. *Front. Microbiol.* **2018**, *9*, 2792.

(11) Celik, E.; Maczka, M.; Bergen, N.; Brinkhoff, T.; Schulz, S.; Dickschat, J. S. Metabolism of 2,3-dihydroxypropane-1-sulfonate by Marine Bacteria. *Org. Biomol. Chem.* **2017**, *15*, 2919–2922.

(12) Durham, B. P.; Boysen, A. K.; Carlson, L. T.; Groussman, R. D.; Heal, K. R.; Cain, K. R.; Morales, R. L.; Coesel, S. N.; Morris, R. M.; Ingalls, A. E.; Armbrust, E. V. Sulfonate-based Networks Between Eukaryotic Phytoplankton and Heterotrophic Bacteria in the Surface Ocean. *Nat. Microbiol.* **2019**, *4*, 1706–1715.

(13) Landa, M.; Burns, A. S.; Durham, B. P.; Esson, K.; Nowinski, B.; Sharma, S.; Vorobev, A.; Nielsen, T.; Kiene, R. P.; Moran, M. A. Sulfur Metabolites that Facilitate Oceanic Phytoplankton–Bacteria Carbon Flux. *ISME J*. **2019**, *13*, 2536–2550.

(14) Saito, N.; Robert, M.; Kochi, H.; Matsuo, G.; Kakazu, Y.; Soga, T.; Tomita, M. Metabolite Profiling Reveals YihU as a Novel Hydroxybutyrate Dehydrogenase for Alternative Succinic Semialdehyde Metabolism in *Escherichia coli*. *J. Biol. Chem.* **2009**, *284*, 16442–16451.

(15) Njau, R. K.; Herndon, C. A.; Hawes, J. W. New Developments in Our Understanding of the β-Hydroxyacid Dehydrogenases. *Chem. Biol. Interact.* **2001**, *130–132*, 785–791.

(16) Zhou, Y.; Wei, Y.; Lin, L.; Xu, T.; Ang, E. L.; Zhao, H.; Yuchi, Z.; Zhang, Y. Biochemical and Structural Investigation of Sulfoacetaldehyde Reductase from *Klebsiella oxytoca*. *Biochem. J.* **2019**, *476*, 733–746.

(17) Peck, S. C.; Denger, K.; Burrichter, A.; Irwin, S. M.; Balskus, E. P.; Schleheck, D. A Glycyl Radical Enzyme Enables Hydrogen Sulfide Production by the Human Intestinal Bacterium *Bilophila wadsworthia*. *Proc. Natl. Acad. Sci. USA* **2019**, *116*, 3171.

(18) Zhou, Y.; Wei, Y.; Nanjaraj Urs, A. N.; Lin, L.; Xu, T.; Hu, Y.; Ang, E. L.; Zhao, H.; Yuchi, Z.; Zhang, Y. Identification and Characterization of a New Sulfoacetaldehyde Reductase from the Human Gut Bacterium *Bifidobacterium kashiwanohense*. *Biosci. Rep.* **2019**, *39*, BSR20190715.

(19) Abayakoon, P.; Epa, R.; Petricevic, M.; Bengt, C.; Mui, J. W. Y.; van der Peet, P. L.; Zhang, Y.; Lingford, J. P.; White, J. M.; Goddard-Borger, E. D.; Williams, S. J. Comprehensive Synthesis of Substrates, Intermediates, and Products of the Sulfoglycolytic Embden–Meyerhoff–Parnas Pathway. *J. Org. Chem.* **2019**, *84*, 2901–2910.

(20) Gauss, D.; Schoenenberger, B.; Wohlgemuth, R. Chemical and Enzymatic Methodologies for the Synthesis of Enantiomerically Pure Glyceraldehyde 3-phosphates. *Carbohydr. Res.* **2014**, *389,* 18–24.

(21) Rougraff, P. M.; Paxton, R.; Kuntz, M. J.; Crabb, D. W.; Harris, R. A. Purification and Characterization of 3-Hydroxyisobutyrate Dehydrogenase from Rabbit Liver. *J. Biol. Chem.* **1988**, *263*, 327–331.

(22) Shoemark, D. K.; Cliff, M. J.; Sessions, R. B.; Clarke, A. R. Enzymatic Properties of the Lactate Dehydrogenase Enzyme from *Plasmodium falciparum*. *FEBS J.* **2007**, *274*, 2738–2748.

(23) Sharma, M.; Mangas-Sanchez, J.; Turner, N. J.; Grogan, G. NAD(P)H-Dependent Dehydrogenases for the Asymmetric Reductive Amination of Ketones: Structure, Mechanism, Evolution and Application. *Adv. Synth. Catal.* **2017**, *359*, 2011–2025.

(24) Kinetic Analysis of Bisubstrate Mechanisms. In *Comprehensive Enzyme Kinetics;* Leskovac, V., Ed.; Springer US, Boston, MA, 2003; pp 171-189.

(25) Schimerlik, M. I.; Cleland, W. W. Inhibition of Creatine Kinase by Chromium. *Nucleotides* **1973**, *248*, 8418–8423.

(26) Dave, K. G.; Dunlap, R. B.; Jain, M. K.; Cordes, E. H.; Wenkert, E. Highly reduced Analogues of the Pyridine Nucleotide Coenzymes: Synthesis of Tetrahydro- and Hexahydronicotinamide Adenine Dinucleotides and Certain of their Derivatives. *J. Biol. Chem.* **1968**, *243*, 1073-1074.

(27) Long, F.; Vagin, A. A.; Young, P.; Murshudov, G. N. BALBES: a Molecular-Replacement Pipeline. *Acta Crystallogr. D* **2008**, *64*, 125–132.

(28) Osipiuk, J.; Zhou, M.; Moy, S.; Collart, F.; Joachimiak, A. X-Ray Crystal Structure of GarR—tartronate Semialdehyde Reductase from *Salmonella typhimurium*. *J. Struct. Funct. Genomics* **2009**, *10*, 249–253.

(29) Yoneda, K.; Sakuraba, H.; Araki, T.; Ohshima, T. Crystal Structure of the NADP+ and Tartrate-bound Complex of l-Serine 3-Dehydrogenase from the Hyperthermophilic Archaeon *Pyrobaculum calidifontis*. *Extremophiles* **2018**, *22*, 395–405.

(30) Lenz, M.; Fademrecht, S.; Sharma, M.; Pleiss, J.; Grogan, G.; Nestl, B. M. New Imine-reducing Enzymes from β-Hydroxyacid Dehydrogenases by Single Amino Acid Substitutions. *Prot. Eng. Des. Select.* **2018**, *31*, 109–120.

(31) Aleku, G. A.; France, S. P.; Man, H.; Mangas-Sanchez, J.; Montgomery, S. L.; Sharma, M.; Leipold, F.; Hussain, S.; Grogan, G.; Turner, N. J. A Reductive Aminase from *Aspergillus oryzae*. *Nat. Chem.* **2017**, *9*, 961–969.

(32) Sharma, M.; Mangas-Sanchez, J.; France, S. P.; Aleku, G. A.; Montgomery, S. L.; Ramsden, J. I.; Turner, N. J.; Grogan, G. A Mechanism for Reductive Amination Catalyzed by Fungal Reductive Aminases. *ACS Catal.* **2018**, *8*, 11534–11541.

(33) Rodríguez-Mata, M.; Frank, A.; Wells, E.; Leipold, F.; Turner, N. J.; Hart, S.; Turkenburg, J. P.; Grogan, G. Structure and Activity of NADPH-dependent Reductase Q1EQE0 from *Streptomyces kanamyceticus*, which Catalyses the R-Selective Reduction of an Imine Substrate. *ChemBioChem* **2013**, *14*, 1372–1379.

(34) Hayward, S.; Berendsen, H. J. C. Systematic Analysis of Domain Motions in Proteins from Conformational Change: New Results on Citrate Synthase and T4 Lysozyme. *Proteins* **1998**, *30,* 144–154.

(35) Stourac, J.; Vavra, O.; Kokkonen, P.; Filipovic, J.; Pinto, G.; Brezovsky, J.; Damborsky, J.; Bednar, D. Caver Web 1.0: Identification of Tunnels and Channels in Proteins and Analysis of Ligand Transport. *Nucleic Acids Res.* **2019**, *47*, W414–W422.

(36) Speciale, G.; Jin, Y.; Davies, G. J.; Williams, S. J.; Goddard-Borger, E. D. YihQ is a Sulfoquinovosidase that Cleaves Sulfoquinovosyl Diacylglyceride Sulfolipids. *Nat. Chem. Biol.* **2016**, *12*, 215–217.

(37) Abayakoon, P.; Jin, Y.; Lingford, J. P.; Petricevic, M.; John, A.; Ryan, E.; Wai-Ying Mui, J.; Pires, D. E. V.; Ascher, D. B.; Davies, G. J.; Goddard-Borger, E. D.; Williams, S. J. Structural and Biochemical Insights into the Function and Evolution of Sulfoquinovosidases. *ACS Cent. Sci.* **2018**, *4*, 1266–1273.

(38) Felux, A.-K.; Spiteller, D.; Klebensberger, J.; Schleheck, D. Entner–Doudoroff Pathway for Sulfoquinovose Degradation in *Pseudomonas putida* SQ1. *Proc. Natl. Acad. Sci. USA* **2015**, *112*, E4298–E4305.

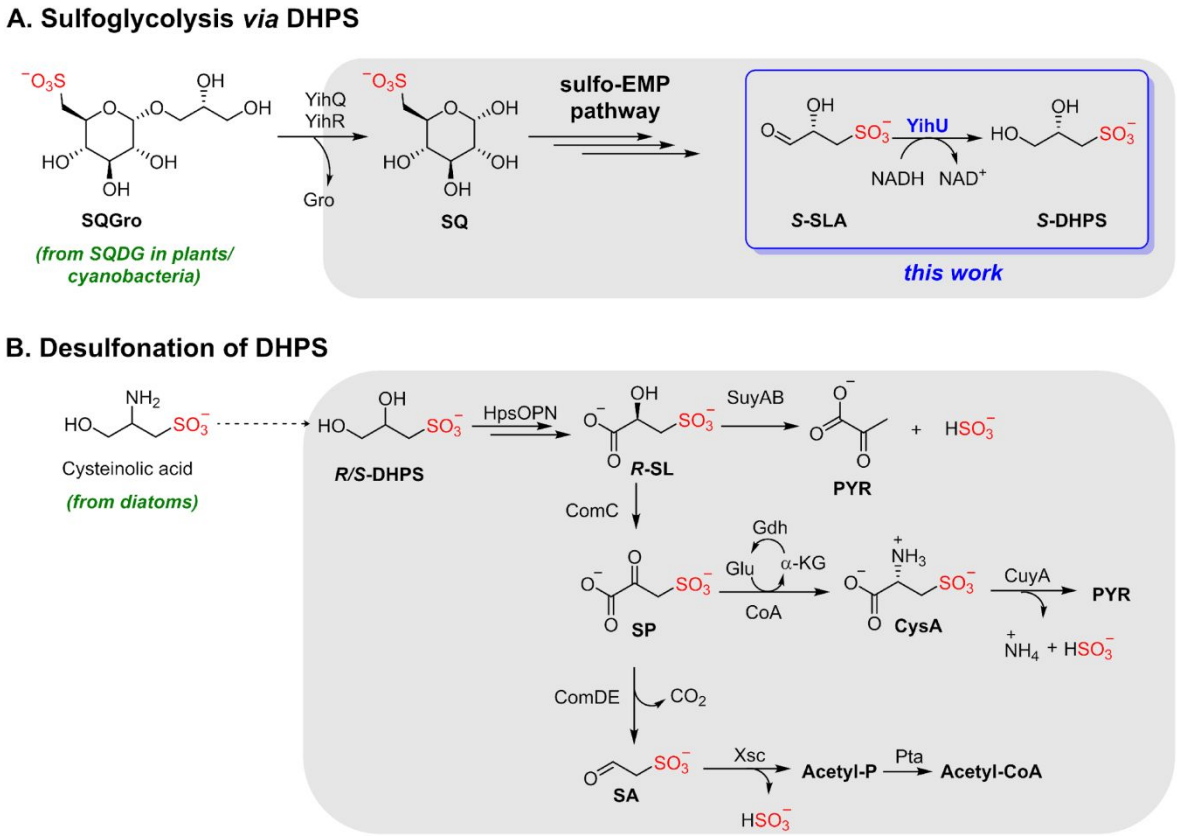

Figure 1. General pathways for cycling of sulfur from organosulfur sources *via* DHPS. *A*, Sulfo-EMP pathway in bacteria for degradation of SQDG to give *S*-DHPS. YihU-catalyzed reduction of SLA to DHPS is shown in blue. *B*, Degradative pathways for mineralization of sulfur from DHPS. Biosynthesis of DHPS by putative deamination of cysteinolic acid is likely catalysed by CoA/ComC homologues.

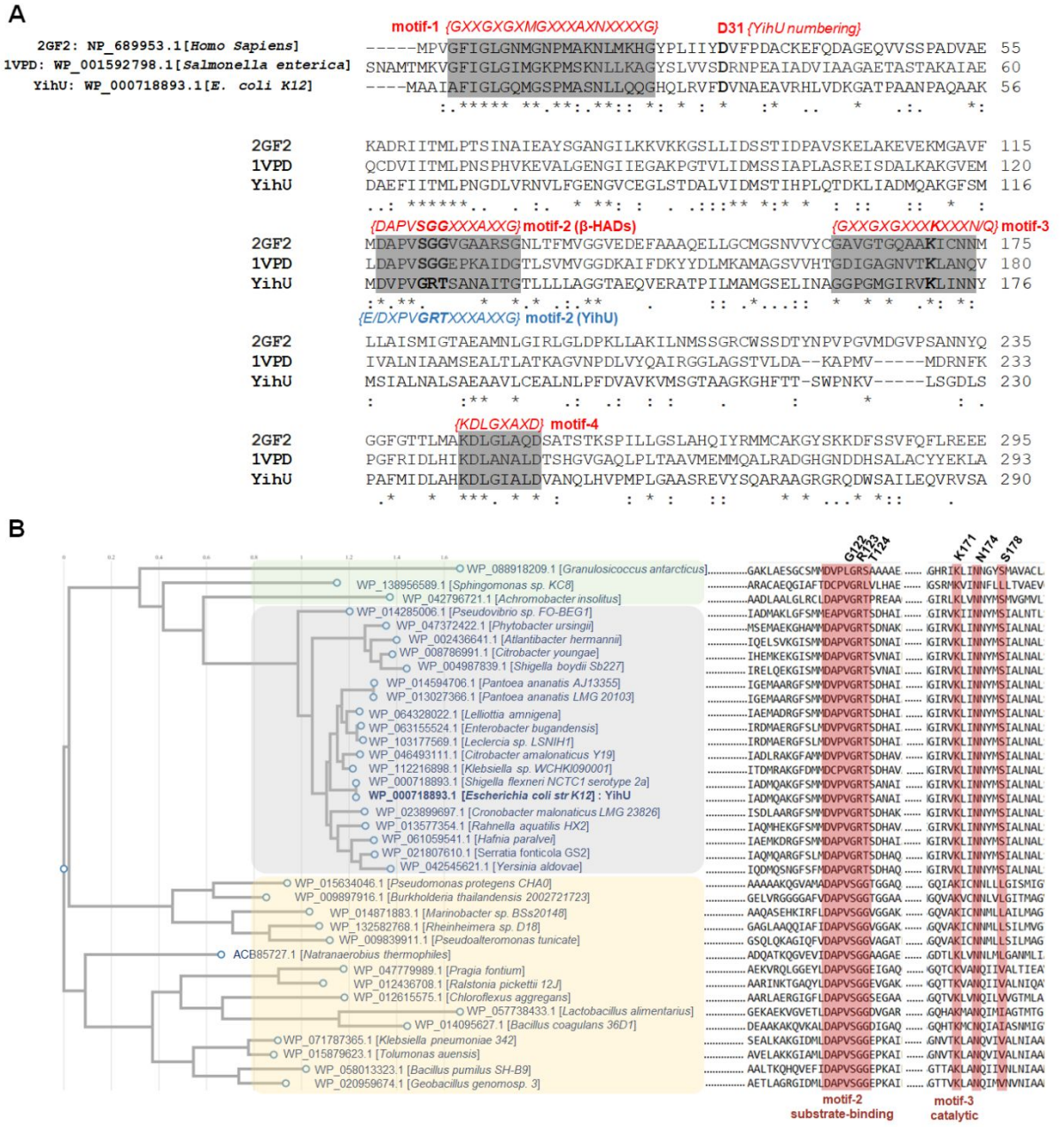

Figure 2. SLA reductases share β-HAD sequence motifs but possess a unique sulfonate substrate binding sequence. A, Sequence alignment of YihU with model β-HADs to show four consensus sequence motifs [motif 1 – cofactor binding *GXXGXG* sequence; motif 2 – substrate binding; motif 3 containing catalytic lysine; motif 4 – cofactor binding]. All four motifs are also conserved in YihU with the only differences in the substrate binding sequence highlighted in motif-2 residues: G122-R123-T124. *B*, Phylogenetic tree showing relationship of SLA reductases (grey box) and β-hydroxy acid dehydrogenases (yellow box); consensus β-HAD sequence motifs for substrate binding motif-2 and catalytic motif-3 are indicated. SLA reductases form a separate sub-group with conserved 'sulfonate substrate binding sequence' at residues 122-124 (YihU numbering). Also highlighted is a clade comprised of other annotated β-HADs with predicted roles in sulfur metabolism (green box).

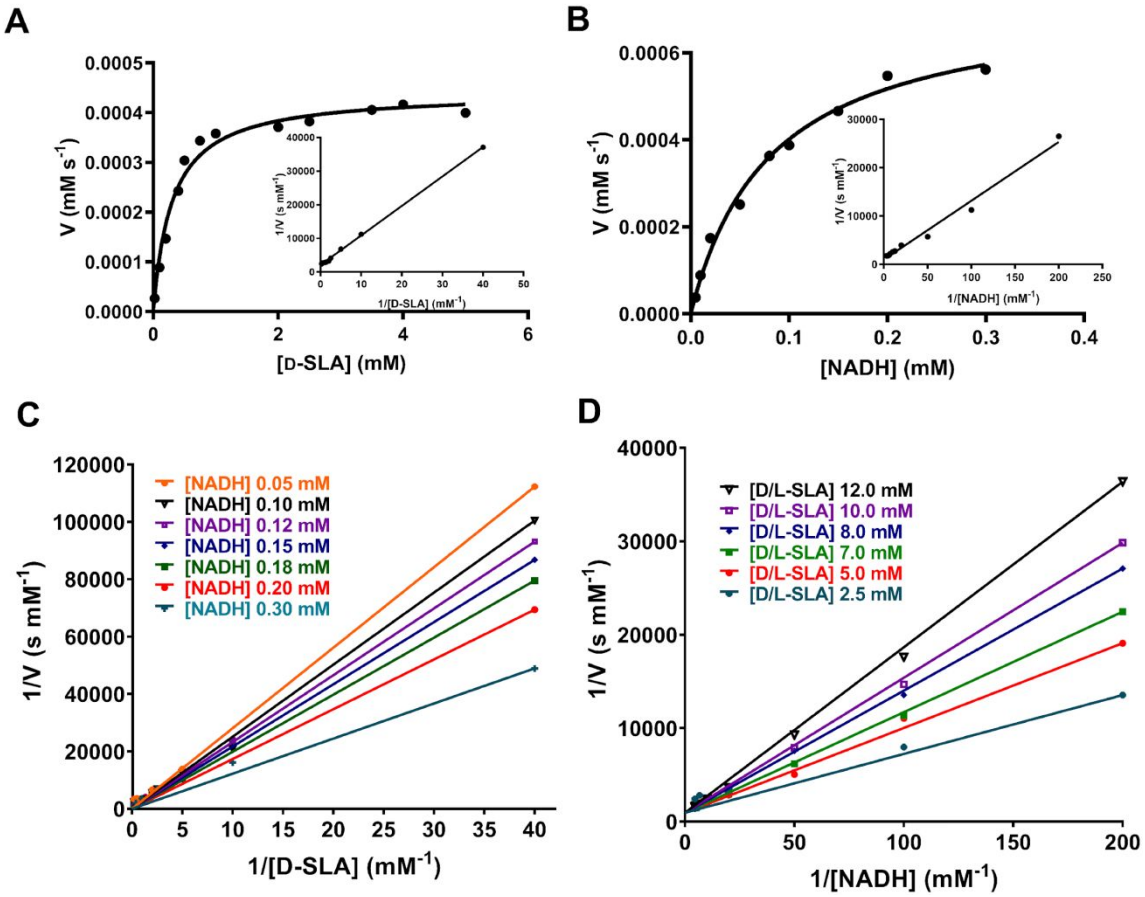

Figure 3. Kinetic studies and double reciprocal plots for rapid equilibrium sequential binding mechanism. *A-B*, Michaelis-Menten and Lineweaver-Burk (inset) plots for reduction of SLA to DHPS by YihU under pseudo first order conditions of [NADH] = 0.1 mM (for A) and [D-SLA] = 2.5 mM (for B). *C-D*, Double reciprocal plots indicate a rapid equilibrium sequential mechanism for YihU. D-SLA concentration was varied at several fixed concentrations of NADH (0.05–0.30 mM). *D*, NADH concentration was varied at several fixed concentrations of DL-SLA (2.5–12.0 mM).

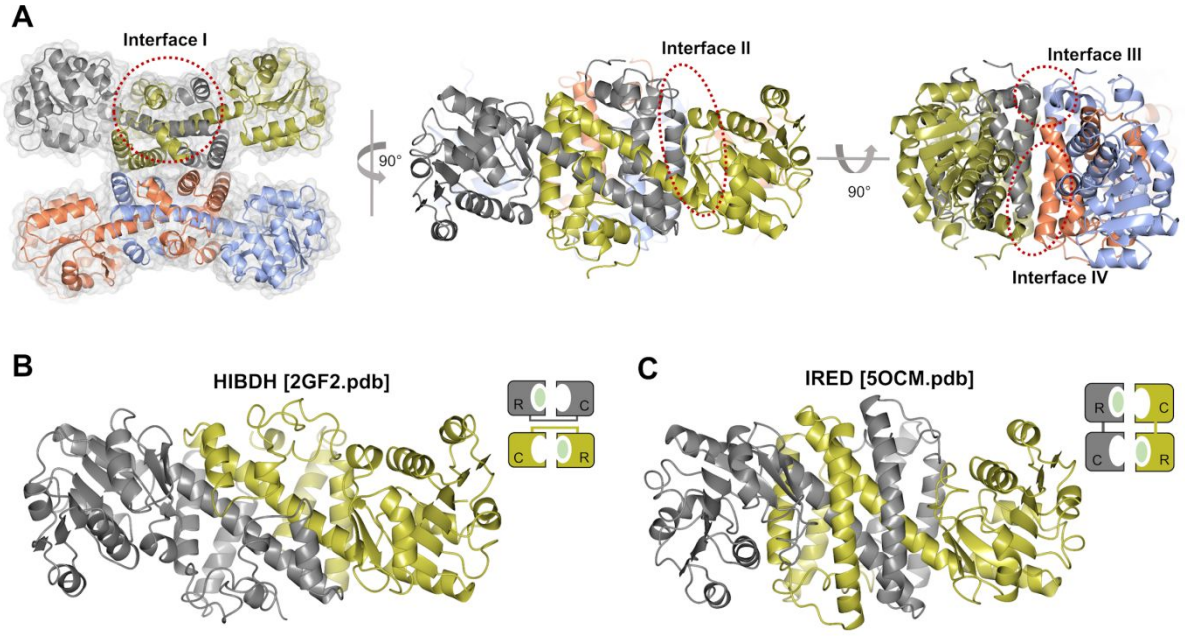

Figure 4. Domain organisation of YihU and comparison with HIBDHs and IREDs. *A*, Overall structure of YihU-apo depicted as dimer-of-dimers in different orientations (related by 90° rotation) to show interfaces I-IV. *B-C,* Representative dimer pairs from crystal structures of human HIBDH (2GF2) and the IRED from *Streptosporangium roseum* (5OCM) showing differences in domain organization between HIBDH *vs.* IRED/YihU enzymes. For each enzyme, the protomers from each dimer pair are depicted in different colours for clarity (in grey and gold or coral and blue).

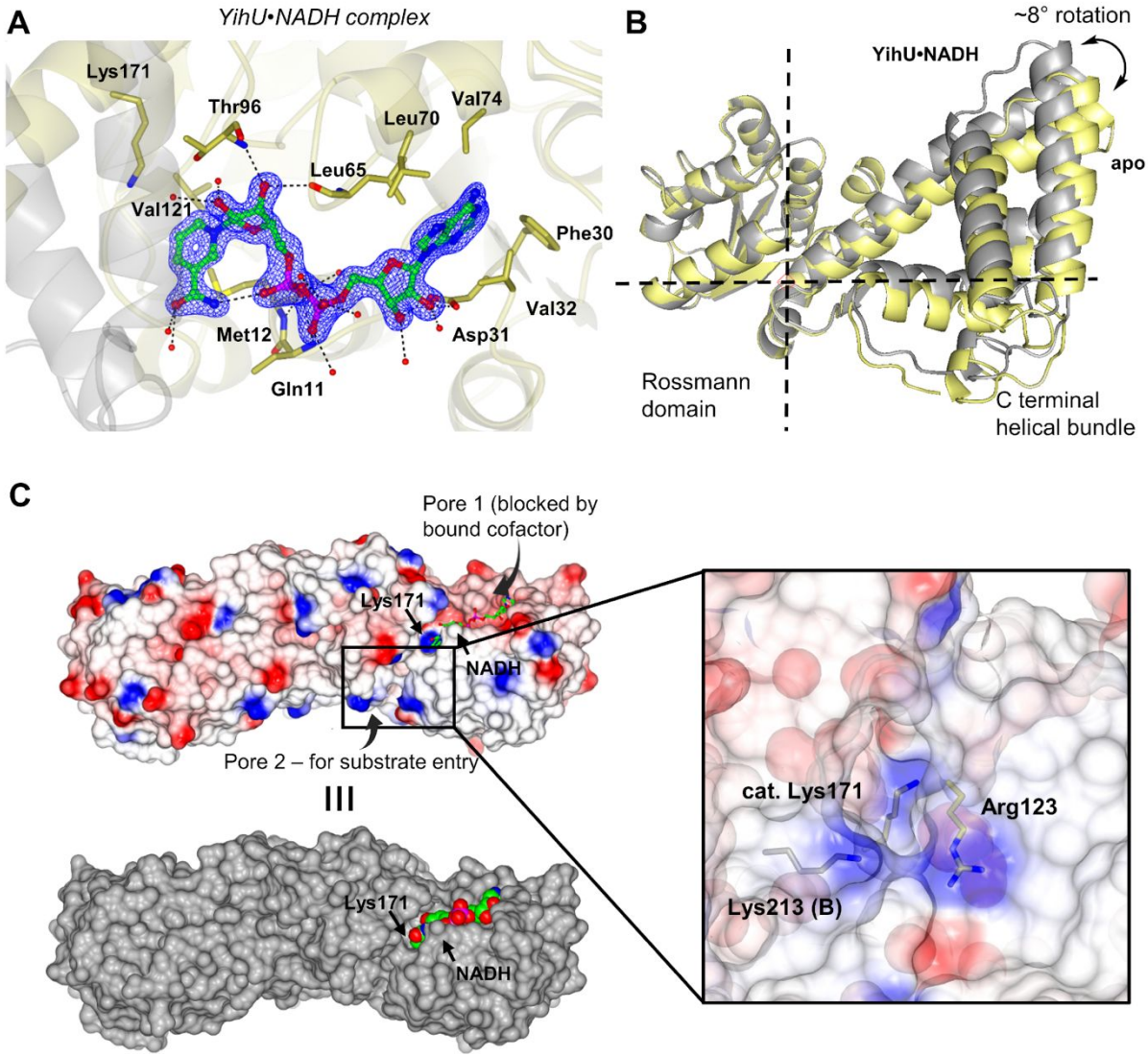

Figure 5. Dynamic domain movements revealed in the complex of YihU•NADH. *A*, Close-up of NADH bound to YihU. Backbone and carbon atoms of subunits A and B are shown in gold and grey, respectively, and NADH and DHPS are shown in cylinder format. Electron density corresponds to the 2Fo − Fc and in blue at levels of 1.5σ. *B*, DynDom analysis of the dynamic domains and hinge bending motion of the YihU-apo (depicted in gold) *vs.* NADH bound conformation (in grey); the lines cross at the centre of rotation and the hinge axis is perpendicular to this crossing point. *C*, Electrostatic potential depiction of YihU-apo dimer surface showing positively charged patch on the surface gated by Arg123 and Lys213. The 'pore' was visualized from surface to catalytic Lys171 in the active site (see Figure S9).

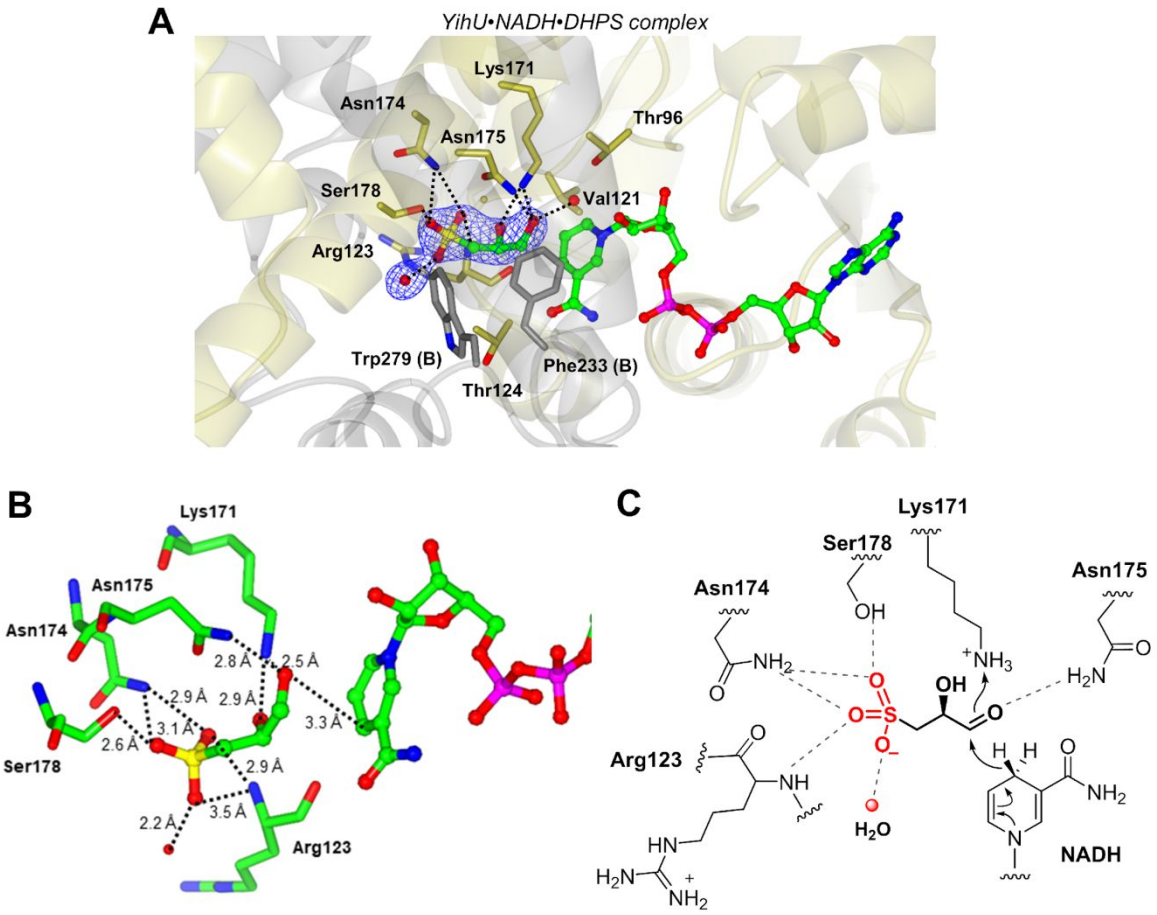

Figure 6. Active site and mechanism of SLA reductase YihU. *A*, Ternary complex structure of YihU with NADH and DHPS bound at the active site showing the sulfonate pocket. Backbone and carbon atoms of subunits A and B are shown in gold and grey, respectively, and NADH and DHPS are shown in cylinder format. Electron density corresponds to the 2Fo − Fc map (in blue) at levels of 1.2σ. *B,* Detailed view of substrate binding pocket of YihU as observed in the ternary complex depicting hydrogen bonding interactions of DHPS with active site residues. *C*, Mechanism of SLA reductases proposed based on YihU•NADH•DHPS crystal structure showing hydride transfer from C4 of the *si*-face of the nicotinamide ring of NADH to the carbonyl of SLA, with lysine-171 as general acid residue.

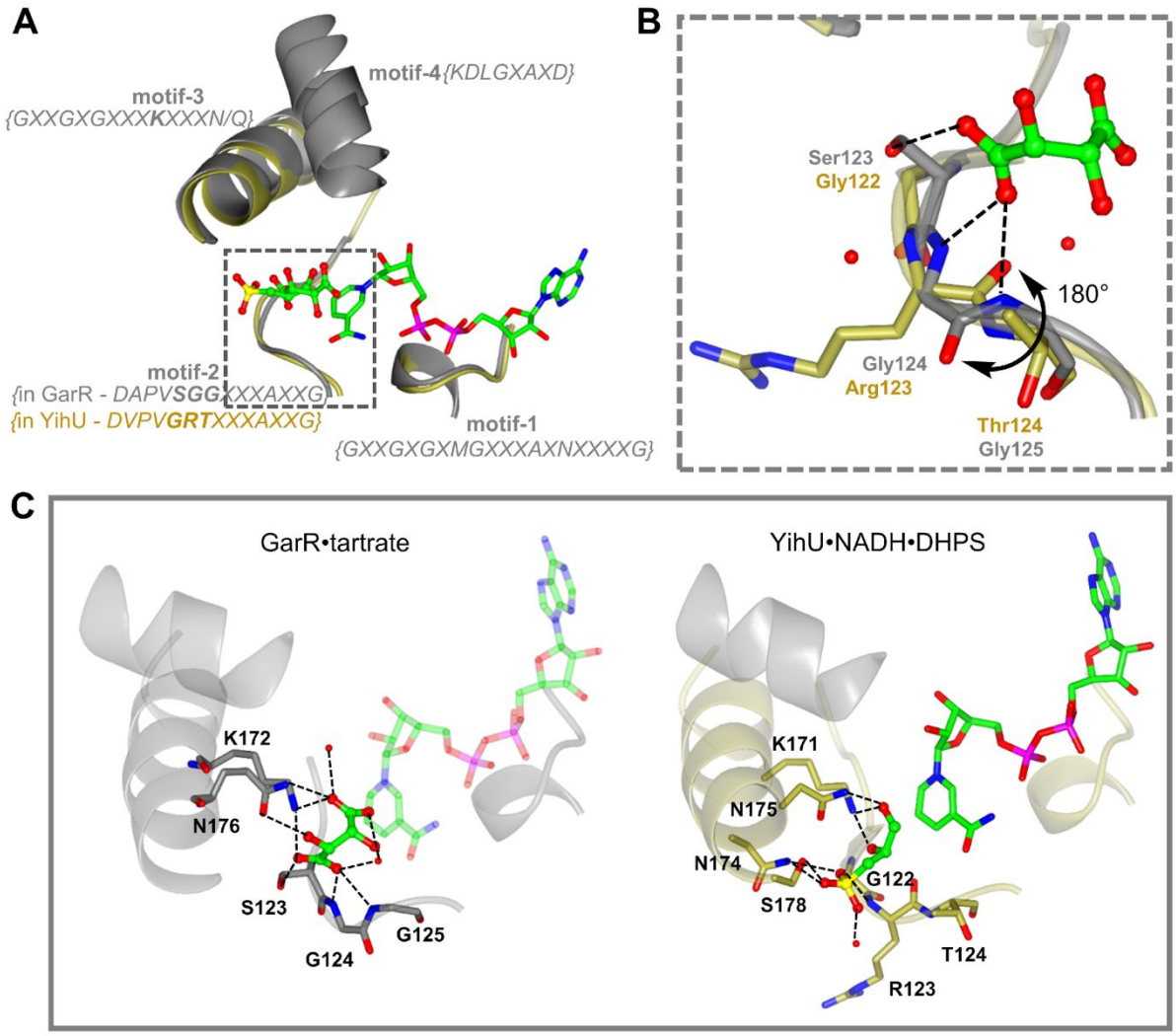

Figure 7. Flexibility in structurally conserved β-HAD motifs provide distinct binding modes for carboxylate versus sulfonate substrates. *A,* Overlay of motifs 1-4 in the YihU•NADH•DHPS dimer pair (in gold and grey) and GarR•tartrate monomer (in grey). *B,* Close-up view of the substrate binding loop containing *DAPV**SGG*** in GarR and *DVPV**GRT*** sequence in YihU showing flip in backbone amides to bind the carboxylate substrate analog, L-tartrate. *C,* Comparison of carboxylate binding site in GarR•tartrate (1VPD) and sulfonate binding site in the YihU•NADH•DHPS structure. The NADH molecule is superposed here from the YihU•NADH•DHPS structure to illustrate the relative positioning of the cofactor in the GarR•tartrate structure.

Table 1. Kinetic parameters for YihU wildtype and mutants of residues in the sulfonate binding site.

Enzyme	Variable substrate	k_{cat} (s^{-1})	K_M^{app} (mM)	k_{cat}/K_M^{app} (mM^{-1} s^{-1})
YihU wildtype	SLA[a]	332 ± 9	0.30 ± 0.038	1090 ± 120
	NADH[b]	548 ± 28	0.082 ± 0.011	6720 ± 580
YihU-G122S	SLA[a]	71 ± 2	1.63 ± 0.11	43 ± 4
	NADH[b]	178 ± 9	0.123 ± 0.013	1450 ± 230
YihU-R123G	SLA[a]	68 ± 6	7.99 ± 1.02	8.5 ± 1.8
	NADH[b]	22.1 ± 0.5	0.009 ± 0.001	2360 ± 300
YihU-T124G	SLA[a]	27 ± 2	5.74 ± 0.79	4.7 ± 1.0
	NADH[b]	12.7 ± 0.6	0.023 ± 0.004	570 ± 130

[a] [SLA] was varied while [NADH] was held constant at 0.1 mM.
[b] [NADH] was varied while [SLA] was held constant at 5 mM.